frontiers | Frontiers in Marine Science

TYPE Original Research
PUBLISHED 04 October 2024
DOI 10.3389/fmars.2024.1462439



OPEN ACCESS

EDITED BY
John S. Armstrong-Altrin,
National Autonomous University of Mexico, Mexico

REVIEWED BY
Lihua Zuo,
Texas A&M University Kingsville, United States
Pibo Su,
Guangzhou Marine Geological Survey, China

*CORRESPONDENCE
Zhifeng Wan
wanzhif@mail.sysu.edu.cn

RECEIVED 10 July 2024
ACCEPTED 16 September 2024
PUBLISHED 04 October 2024

CITATION
Wu X, Shi C, Guo F, Li Z, Luo J, Li P, Wang Z, Wang G and Wan Z (2024) Provenance and transport mechanism of marine sediments in the Zhongjiannan Basin.
*Front. Mar. Sci.* 11:1462439.
doi: 10.3389/fmars.2024.1462439



# Provenance and transport mechanism of marine sediments in the Zhongjiannan Basin

Xuewan Wu[1], Chaoqi Shi[1], Feng Guo[2], Zihan Li[1], Junsheng Luo[1], Peipeng Li[1], Ziwen Wang[3], Guifeng Wang[3] and Zhifeng Wan[1]*

[1]Southern Marine Science and Engineering Guangdong Laboratory, School of Marine Sciences, Sun Yat-Sen University, Zhuhai, China, [2]Guangdong Provincial Marine Geological Survey Institute, Guangzhou, China, [3]Key Laboratory of Marine Geological Resources and Environment, Hainan Provincial Marine Geological Survey Institute, Haikou, China

The research on the source of marine sediments has a vital impact on identifying material sources, transport mechanism, and the evolution of sedimentary environments. Previous studies have shown many outstanding achievements on the source analysis of the South China Sea, but there are still some controversies over the complex source and transport mechanisms of the Zhongjiannan Basin. In this study, we took a gravity core (583cm) from the Zhongjiannan Basin and analyzed the particle size, rare earth elements, and Sr-Nd isotopes of the core sediments to further reveal the source and transport mechanism. The surface sediments in the Zhongjiannan Basin were relatively stable, with an average particle size ranging from 5.66 to 17.74 μm. The normalized standard curve of chondrite exhibited the depletion of Eu, with LREE dominated in REE. As the depth increased, $^{87}Sr/^{86}Sr$ ratios showed a gradually increasing trend, while δNd change was relatively complex. On the whole, $^{87}Sr/^{86}Sr$ ratios (from 0.721537 to 0.725322) and δNd (from -11.561617 to -12.289374) were in a relatively narrow range. Based on the particle size characteristics, we found the geochemical characteristics of sediment largely resulted from different sediment sources. By comparing rare earth elements and Sr-Nd isotopes, we concluded the sediment of the Zhongjiannan Basin was from mainly terrigenous contribution. In addition, taking into account factors such as terrain, migration distance, and river drainage system, we conclude the sediment were mainly from the Mekong River, the Red River, Taiwan Island, and Hainan Island. The surface current along the northeast direction was the main transportation route for the sediments of the Mekong River. The Guangdong coastal current and the southwest surface current transported sediment from the Red River and Hainan Island to the Zhongjiannan Basin. The surface current and deep-water current in the southwest direction carried sediment from Taiwan Island to the study area, while the Kuroshio also had some impacts on the sediment transportation of Taiwan Island. This study has reinforced the research on provenance in the South China Sea Basin and has an important significance on evolution of sedimentary environments, evolution of ancient oceans.

KEYWORDS

**Zhongjiannan Basin, provenance, transport mechanism, Sr-Nd isotope, rare earth elements**

# 1 Introduction

The marginal sea is a crucial transition zone connecting land and the deep sea, making it an ideal region for investigating land-ocean interactions, where sediment budgets and transport mechanism can more easily be quantitatively defined (Hu et al., 2022). Marginal sea sediments play an important role in continental uplift, continental denudation, climate change and paleo-ocean evolution (Syvitski, 2003; Yang et al., 2003; Kuehl and Nittrouer, 2011). Therefore, it is critical to clarify the source of marginal sea sediments. As the largest marginal sea in the Western Pacific, the South China Sea (SCS) has a large number of sediment sources, which are controlled by various complex factors. Approximately 1600 million tons (Mts) of river sediment are discharged into the SCS every year from many surrounding rivers, accounting for 80% of the sediment input to the SCS, with the vast majority of sediment supply coming from land and islands. Previous studies have conducted extensive research on the sediments in the SCS, including mineral composition analysis, major and trace element analysis, single mineral dating analysis, and Sr-Nd isotope analysis, and all have achieved outstanding results (Yang et al., 2007; Wei et al., 2012; Liu et al., 2018; Hu et al., 2022; Qiu et al., 2022). The most of sediments in the northern South China Sea (NSCS) come from the Taiwan River (176 Mts/yr), the Pearl River (102 Mts/yr) and the Red River (138 Mts/yr). In addition, the sediment transport rate from the Mekong River to the SCS is as high as 166Mts/yr. Terrigenous sediments in the northeastern SCS derive mainly from the Pearl River, rivers in southwestern Taiwan, and rivers in Luzon, which include the Taixi Basin, the Taixinan Basin, the Pearl River Mouth Basin, and the Zhongjiannan Basin (Liu et al., 2008). The sediments of the deep-water area in Qiongdongnan Basin are mainly from the sources of the Red River, Taiwan, Pearl River, Hainan Island, and Vietnam (Huang et al., 2023). The Red River and Hainan are the major sources of the sediments on the Yinggehai Basin, with minor contributions from central Vietnam (Wang et al., 2019). Gong et al., 2021 demonstrated that sediments of Beibuwan Basin were uniformly derived from the Yunkai Massif and Hainan Island in the middle-upper Eocene. In the southern South China Sea (SSCS), river sediment inputs mainly come from rivers in the Malay Peninsula, Sumatra, and Borneo (Milliman et al., 1999). These sediments enter the basins under the action of ocean currents, such as the Zengmu Basin, Wan'an Basin, and Mekong Basin. Marine sediment sources and transport are influenced by river flows, sea level changes, and tectonic movements (Cai et al., 2020). Due to the different material compositions of river sediments flowing into the SCS, different source-sink processes lead to diverse geochemical characteristics. Therefore, the complexity of sedimentary processes determines that a single geochemical proxy cannot accurately indicate the source of sediments. On the contrary, a variety of methods should be used. Previous studies have shown that the mixing of strong surface currents in the western and southern parts of the SCS results in the high uniformity of four major clay minerals (illite, montmorillonite, chlorite, and kaolinite) (Liu et al., 2016b). Therefore, the mineral composition alone does not clearly determine the source of the large amount of sediment in SCS (Wei et al., 2012). Because rare earth elements (REEs) are mainly transported and deposited in particulate form in seawater, its composition changes little during rock weathering and transportation, and the source rock information it carries is well reserved. Therefore, REE is an important source tracer (Kimoto et al., 2006; Stevens and Quinton, 2008; Huang et al., 2023). Nd isotope characteristics show a banded distribution and are very consistent with Nd isotope composition of the sediment provided by the river system flowing into the corresponding area, indicating that the Nd isotope composition is a convincing evidence for the source of SCS sediment (Wei et al., 2012). However, there are still some controversies regarding the source of sediments in the central SCS. Previous research has shown that the sediment in the Zhongjiannan Basin is greatly influenced by the Beibu Gulf and the Red River (Wei et al., 2012), but the studies by Deng et al., 2021; Cai et al., 2022 show that the sediments in the southwestern subbasin of the SCS are mainly derived from Taiwan and the Mekong River.

There are continuous and sufficient sediment records in the SSCS, which can record important information such as the evolution of the East Asian monsoon, the sources of marine sediments, and the ancient productivity of the SCS. Therefore, SSCS is an ideal area for studying paleoclimate change and sedimentary environment evolution since the late Miocene (Chen et al., 2003; Wan et al., 2006; Zhang et al., 2009). In this study, we analyzed the particle size, REEs and Sr-Nd isotopes of sediments collected in a sedimentary gravity core from the Zhongjiannan Basin in the SSCS, compared and analyzed the effects of different river inputs on sediment sources, and discussed the corresponding transport mechanism. This study enriches the study of provenance in the SCS Basin and contributes to the application of the geochemical methods in provenance tracing.

# 2 Geological setting

The SCS is a large continental margin basin located at the intersection of the Eurasian Plate, the Pacific Plate and the Indo-Australian Plate, with complex interactions and tectonic conditions (Morley, 2012). Studies on ocean drilling have found that the SCS opened from the east along a strike-slip fault, then extended west along an extended ridge, and finally disappeared due to the Manila subduction, which caused the formation of the ocean crust to the east. Research has shown that the SCS ocean bottom began to subduct northward at~125 Ma ago, leading to post-arc extension along the southern edge of the Eurasian plate and the formation of the original SCS. During the Late Cretaceous, the subduction of mountain ridges led to changes in the subduction mechanism of the Neotethys, forming fold zones, uplifts, erosion, and extensive unconformities (Li et al., 1999). The natural area of the SCS is about 3.5 million square kilometers, which is the largest and deepest sea area in China's coastal waters. In addition, the average depth of SCS is 1,212 meters, with a maximum depth of 5,559 meters. The main rivers that flow into the SCS are the Pearl River, the Red River and the Mekong River. The SCS receives approximately 700 Mts of river sediments annually from surrounding islands, which results in consistently stable sedimentation at a relatively high rate (Qiu et al., 2022).

The Zhongjian Basin is a stretching basin formed in a north-south trend, located south of the Qiongdongnan Basin and west of the Xisha Sea. It is accompanied by strong and large-scale magmatic activity under the combined influence of the north-east continental margin extension system and the strike-slip system. The Zhongjiannan Basin has complex

geological characteristics, which are not only controlled by the interaction between the Pacific, India Australia, and Eurasian plates, but also influenced by SCS seafloor diffusion (Dimitrov, 2002; Wan et al., 2019). There are many igneous rocks and developed faults in the Zhongjiannan Basin, including extensional, transitional, and compressive shear faults (Fyhn et al., 2009). Due to the development of a large number of rivers, alluvial fans, and lacustrine facies, the surface of the basin is covered by a thick layer of fine-grained sediments (Wan et al., 2019). Since the late Miocene, the sedimentary and tectonic evolution of the Zhongjiannan Basin has been mainly controlled by the residual magmatic activity after the expansion of the southwest subbasin stopped. The extrusion tectonic stress field gradually weakens from south to north, and the evolution of sedimentary structure depends on two different tectonic stress fields (Yin et al., 2023).

# 3 Samples and methods

## 3.1 Samples

The samples were obtained from the continental slope in the Zhongjiannan Basin using the "Jiageng Hao" of the Xiamen University during the scientific expedition voyage (the National Natural Science Foundation of China Shared Voyage Program "Experimental Study on the 2021 Central South China Sea Basin Scientific Survey of the Shared Voyage Plan"). The location of the gravity core in the study area is shown in Figure 1. The Z18 (13°44′ 20.76″N, 112°9′9.72″E, total length 593cm) sediment core was collected in the deep-water area of the central SCS. The samples are loose sediments of unformed rocks and are grayish-brown in color. The mineral phases at different depths are almost identical, mainly calcite and quartz and clay minerals (e.g., illite), with more calcite in the shallower horizons (Supplementary Figure S1). The sediments are fine-grained and may contain silt to fine sand level particles. Core sediments were cut into 5 cm long slices using a wooden knife, and in-situ packed into plastic bags.

## 3.2 Methods

Particle size testing was conducted on samples. We took samples every five centimeters and a total of 116 particle size samples were obtained. The sediment particle size test was completed at the Southern Marine Science and Engineering Guangdong Laboratory (Zhuhai) using the Mastersizer3000 laser particle size analyzer produced by Malvern Company in the UK. The pre-treatment method was as follows: 15 mL of 30% $H_2O_2$ solution was added to 0.2g of sediment sample. Reacted for 12 hours to remove organic matter. Then 15 mL of dilute hydrochloric acid was added. Reacted in a 40°C water bath for 24 hours to remove biological carbonates. All the analyses were performed with 15-21% obscuration, 2500 rpm stirrer speed, continuous ultrasound in this study. After machine testing, the average particle size (Mz) and sorting coefficient were calculated using the formulas proposed by Folk and Ward for the measured data (σ), Particle size parameters such as skewness (Sk) and kurtosis (Kg) (Jaijel et al., 2021).

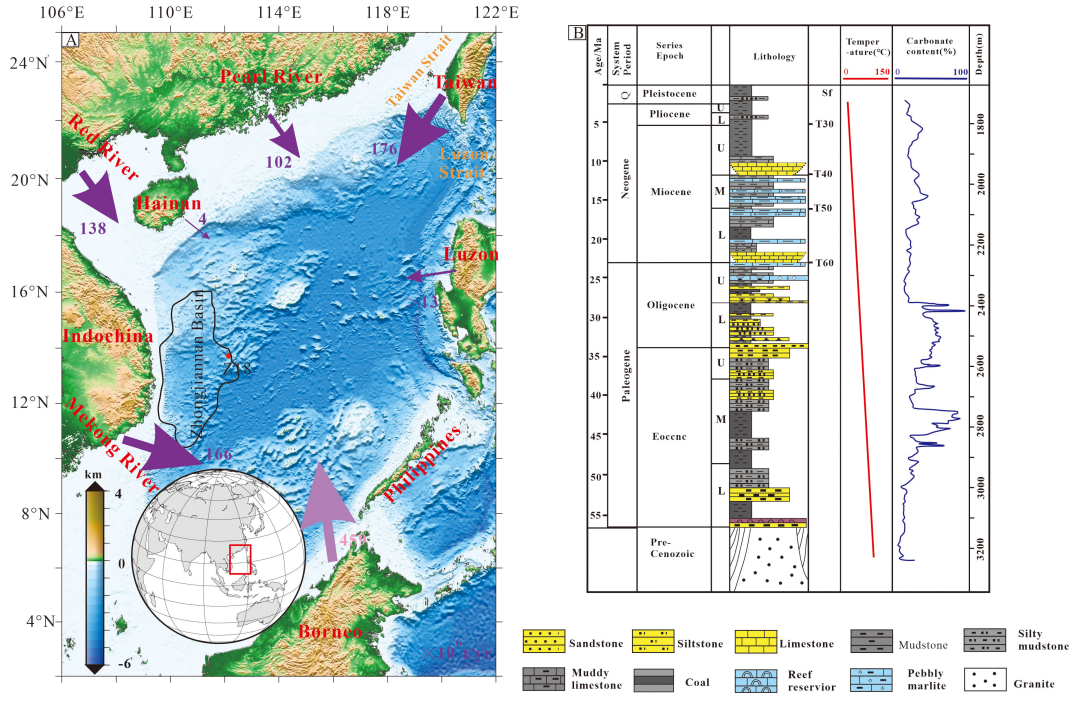


FIGURE 1
**(A)** Map showing the locations, topography of Core Z18 and the annual suspended sediment discharge of fluvial drainage systems in the SCS. (modified from Liu et al., 2016b; Cai et al., 2020; Geng et al., 2020; Cai et al., 2022; Huang et al., 2023). **(B)** Tectonic chronostratigraphic graph of the Zhongjiannan Basin (Geng et al., 2020; Wang et al., 2024).

The analysis of REEs was done at the ALS Minerals-ALS Chemex. We took samples every twenty centimeters and total of 29 samples were obtained. The analysis of REEs was as follows: added lithium borate ($LiBO_2/Li_2B_4O_7$) to the samples, mixed evenly, and melted in a furnace at 1025°C. After the molten solution cooled down, we digested them with nitric acid ($HNO_3$), hydrochloric acid (HCl), and hydrofluoric acid (HF) to a constant volume. 100 µL solutions were extracted and added with 10 mL 2% $HNO_3$ for major elements measurement, while 60 µL solutions were extracted and added with 3 mL 2% $HNO_3$ for trace elements measurement, which were all precisely weighed. The sample solutions were analyzed on Agilent 7700 inductively coupled plasma mass spectrometry (ICP-MS). The relative deviation and relative error of REEs were less than 10%.

For Sr and Nd isotopic measurements, we took samples every sixty centimeters and a total of 9 samples were obtained. Authigenic carbonates in the sample were removed using 30% hydrochloric acid. And then we used a muffle furnace to remove organic matter at 600° C, then weighed about 100mg of powder samples and placed them in a Teflon digestion tank. Nitric acid and hydrofluoric acid were sequentially added, and placed in an oven at 190°C for 48 hours. We took the supernatant for Sr-Nd isotope separation. Sr isotopes were separated and purified using Sr spec resin, while Nd isotopes were purified using LN resin. Experimental preprocessing, and Sr-Nd isotopic measurements were completed in the super-clean laboratory of S Southern Marine Science and Engineering Guangdong Laboratory (Zhuhai). The Sr isotopic measurements were performed on Thermal Ionization Mass Spectrometer (TIMS) and the Nd isotopic measurements were performed on a multi-collector mass spectrometer (MC-ICP-MS). The JNdi-1 and the NBS987-1 standards were repeatedly measured to monitor the precision and accuracy of the determinations. The Nd isotopic results are also expressed as $\varepsilon Nd = [(( ^{143}Nd/^{144}Nd_{meas})/0.512638)-1] \times 10000$, using the Chondritic Uniform Reservoir value given by Jacobsen and Wasserburg (1980).

# 4 Result

## 4.1 Grain size variations

The mean size of sediments ranged from 5.66 to 17.74 µm (average 11.19 µm), while the median particle size ranged from 2.75 to 6.93 µm (average 4.98 µm). Clay (<4 µm) content ranged from 27.98 to 66.81%, with silt (4-63 µm) content ranged from 31.97% to 69.09%, with sand (>63 µm) content ranged from 0.93 to 8.46% (Figure 2, Table 1, and more data can be found in Appendix S1). The sediments mainly consisted of clay and silt, with a relatively small content of sand, The clay contents in deeper sediments were higher than that in shallower sediments, while the sand contents were exactly the opposite. Overall, the sediment particles were small. The skewness ranged from 3.18 to 6.76, and these positive values indicated that larger sediment particles accounted for the main proportion. As the depth increased, both skewness and kurtosis showed a gradually increasing trend.

## 4.2 Concentrations and spatial characteristics of REEs

The mean ΣREE of surface sediments was 185.60 µg/g, with a minimum and maximum value of 158.61 and 217.19 µg/g in the Z18 site (Table 2). Besides, the light REEs (LREEs, from La to Eu) showed a mean value of 143.80µg/g while the mean value of heavy REEs (HREEs, from Gd to Lu) was 41.81µg/g (Table 2). LREE contributed the main part of REEs (Figure 3). The LREEs/HREEs values ranged from 3.29 to 3.63 with an average value of 3.43 (Table 2). As the depth increased, the ΣREE showed an increasing trend overall in the vertical variation characteristics of ΣREE (Table 2). The mean values of $(La/Yb)_N$, $(La/Sm)_N$, $(Gd/Yb)_N$ were respectively 10.37, 3.77, 1.83 in the Z18 site (Table 2, N is the normalization to chondrite).

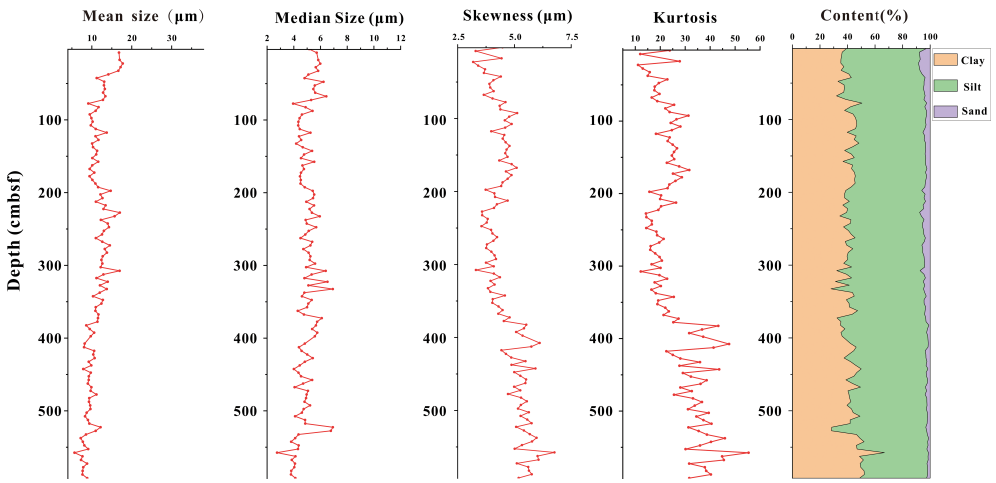


FIGURE 2
Variations of mean size, medial size, skewness, kurtosis, material composition at the core Z18.

10.3389/fmars.2024.1462439

TABLE 1 Clay Content, Silt Content, Sand Content, Median Size and Mean Size of the sediment of different depths.

| Depth(cmbsf) | - | Clay Content (%) | Silt Content(%) | Sand Content(%) | Median Size (μm) | Mean Size (μm) |
|---|---|---|---|---|---|---|
| 0-100 | Maximum | 50.48 | 64.29 | 8.46 | 6.44 | 17.74 |
| | Minimum | 32.02 | 47.00 | 2.52 | 3.95 | 9.12 |
| | Average | 38.90 | 56.25 | 4.85 | 5.36 | 13.18 |
| 100-200 | Maximum | 48.28 | 59.98 | 6.13 | 5.53 | 14.72 |
| | Minimum | 36.74 | 48.44 | 2.34 | 4.18 | 9.42 |
| | Average | 43.68 | 52.71 | 3.60 | 4.70 | 10.93 |
| 200-300 | Maximum | 45.52 | 59.17 | 7.67 | 5.95 | 17.00 |
| | Minimum | 34.40 | 50.77 | 3.38 | 4.50 | 11.00 |
| | Average | 39.85 | 55.26 | 4.89 | 5.22 | 13.19 |
| 300-400 | Maximum | 47.32 | 67.20 | 7.35 | 6.92 | 16.96 |
| | Minimum | 27.98 | 48.99 | 0.93 | 4.30 | 8.61 |
| | Average | 38.52 | 57.81 | 3.66 | 5.40 | 11.76 |
| 400-500 | Maximum | 49.94 | 59.48 | 3.69 | 5.42 | 11.16 |
| | Minimum | 37.47 | 47.08 | 1.38 | 4.00 | 7.85 |
| | Average | 43.18 | 54.25 | 2.57 | 4.75 | 9.51 |
| 510-593 | Maximum | 66.81 | 69.09 | 3.16 | 6.93 | 12.18 |
| | Minimum | 28.41 | 31.97 | 1.17 | 2.75 | 5.66 |
| | Average | 47.03 | 51.00 | 1.97 | 4.40 | 8.46 |
| 0-593 | Maximum | 66.81 | 69.09 | 8.46 | 6.93 | 17.74 |
| | Minimum | 27.98 | 31.97 | 0.93 | 2.75 | 5.66 |
| | Average | 41.83 | 54.57 | 3.60 | 4.98 | 11.19 |

## 4.3 Sr and Nd isotopes

The results of Sr and Nd isotopes were shown in Table 3 and Figure 3. The $^{87}Sr/^{86}Sr$ ratios varied from 0.721537 to 0.725322, with a mean value of 0.723722 in Z18, which were typical values for mixed terrestrial detritus (>0.711) and biogenic carbonate (~0.7092). The $^{143}Nd/^{144}Nd$ ratios varied from 0.512008 to 0.512045, with a mean value of 0.512023. The εNd values showed a very narrow range, -12.2894 to -11.5676 (mean to -11.9968) in Z18 site. As the depth increased, $^{87}Sr/^{86}Sr$ ratio showed a gradual uplift, while the change of δNd were relatively complex.

# 5 Discussion

## 5.1 The relationship among particle size, sedimentary environment, and provenance

The particle size characteristics can well reflect different sources and transport mechanisms (Lim et al., 2006; Meyer et al., 2011). The mean size of sediments ranged from 5.66 to 17.74 μm (average 11.19 μm), which is similar to the particle size characteristics of typical deep-sea sediments (with an average particle size of 7-10 μm) (Feng et al., 2021). In terms of the variations of average particle size at different depths, the particle size at Z18 site is relatively small and stable, with small oscillations. As the depth increases, the average particle size and median particle size show a nearly linear decrease trend (Figure 2). The content of clay, silt, and sand also changes less with depth (Figure 2). We speculate that the surface sediments in Zhongjiannan Basin is relatively stable, which is because that the Z18 site is not located at the mouth of a large-flow river. In addition, due to the impact of sea level fluctuations on sediment transport distance, particle size may also be affected by sea level change (Clift et al., 2014). Huang et al., 2023 proposed that the peak of the average particle size curve indicated that there is a sudden change of hydrodynamic conditions during the sedimentation process. The sediments at Z18 site experience changes of hydrodynamic conditions over a period of time, but the changes are not obvious. The particle size distribution curves of sediments at different depths shows obvious bimodal at 0.7-1.0 μm and 3-8 μm, and some samples have a small protrusion near the 100 μm (Figure 4), indicating that the provenances of the sediment in Zhongjiannan Basin are mixed sources.

In addition, there is no significant correlation between sediment mean size with HREEs/LREEs ($R^2$ = 0.072, n=29), $(La/Yb)_N$ ($R^2$ = 0.248, n=29), $(La/Sm)_N$ ($R^2$ = 0.024, n=29), δCe/δEu ($R^2$ = 0.013, n=29), $^{87}Sr/^{86}Sr$ ($R^2$ = 0.139, n=9), $^{143}Nd/^{144}Nd$ ($R^2$ = 0.013, n=9)

TABLE 2 The abundance of REE in Z18 core sediments (depth from 0-585 cmbsf) (μg/g).

| Depths (cmbsf) | La | Ce | Pr | Nd | Sm | Eu | Gd | Tb | Dy | Ho | Er | Tm | Yb | Lu |
|---|---|---|---|---|---|---|---|---|---|---|---|---|---|---|
| 0-5 | 29.80 | 59.60 | 6.91 | 25.80 | 4.79 | 0.97 | 4.37 | 0.69 | 3.98 | 0.80 | 2.16 | 0.33 | 2.07 | 0.32 |
| 20-25 | 28.10 | 57.20 | 6.60 | 24.60 | 4.58 | 0.95 | 4.24 | 0.68 | 3.91 | 0.78 | 2.15 | 0.31 | 2.09 | 0.32 |
| 40-45 | 29.60 | 60.90 | 7.10 | 25.50 | 5.13 | 1.08 | 4.70 | 0.72 | 4.15 | 0.79 | 2.22 | 0.34 | 2.08 | 0.33 |
| 60-65 | 29.70 | 62.10 | 7.13 | 26.00 | 5.31 | 1.05 | 4.58 | 0.70 | 4.14 | 0.78 | 2.23 | 0.33 | 2.05 | 0.33 |
| 80-85 | 32.50 | 67.70 | 7.69 | 27.50 | 5.57 | 1.11 | 4.71 | 0.73 | 4.24 | 0.82 | 2.38 | 0.34 | 2.16 | 0.34 |
| 100-105 | 33.40 | 68.90 | 8.00 | 29.20 | 5.83 | 1.19 | 5.20 | 0.78 | 4.57 | 0.87 | 2.55 | 0.37 | 2.27 | 0.36 |
| 120-125 | 33.40 | 70.20 | 8.10 | 29.10 | 5.80 | 1.19 | 5.15 | 0.78 | 4.73 | 0.89 | 2.63 | 0.38 | 2.33 | 0.37 |
| 140-145 | 34.40 | 68.90 | 8.18 | 29.20 | 5.94 | 1.19 | 5.18 | 0.78 | 4.55 | 0.88 | 2.50 | 0.37 | 2.33 | 0.36 |
| 160-165 | 34.40 | 69.30 | 8.14 | 28.90 | 5.83 | 1.24 | 5.30 | 0.81 | 4.72 | 0.90 | 2.60 | 0.38 | 2.39 | 0.37 |
| 180-185 | 33.30 | 67.90 | 7.81 | 28.10 | 5.81 | 1.19 | 5.15 | 0.79 | 4.53 | 0.87 | 2.48 | 0.38 | 2.31 | 0.35 |
| 200-205 | 31.00 | 62.50 | 7.40 | 26.40 | 5.30 | 1.11 | 4.74 | 0.74 | 4.28 | 0.83 | 2.40 | 0.36 | 2.18 | 0.35 |
| 220-225 | 31.80 | 64.10 | 7.48 | 27.20 | 5.44 | 1.19 | 5.02 | 0.77 | 4.47 | 0.84 | 2.52 | 0.36 | 2.28 | 0.36 |
| 240-245 | 31.20 | 62.60 | 7.29 | 26.60 | 5.32 | 1.13 | 4.73 | 0.74 | 4.30 | 0.81 | 2.40 | 0.36 | 2.18 | 0.35 |
| 260-265 | 32.30 | 64.90 | 7.73 | 27.80 | 5.59 | 1.19 | 5.07 | 0.76 | 4.51 | 0.87 | 2.50 | 0.36 | 2.29 | 0.37 |
| 280-285 | 31.40 | 64.60 | 7.62 | 27.20 | 5.38 | 1.17 | 4.97 | 0.77 | 4.45 | 0.85 | 2.48 | 0.36 | 2.23 | 0.35 |
| 300-305 | 29.60 | 61.20 | 7.13 | 25.40 | 5.10 | 1.05 | 4.61 | 0.72 | 4.23 | 0.80 | 2.35 | 0.34 | 2.12 | 0.33 |
| 320-325 | 30.10 | 62.40 | 7.22 | 25.80 | 5.18 | 1.04 | 4.53 | 0.68 | 4.07 | 0.77 | 2.23 | 0.33 | 2.06 | 0.33 |
| 340-345 | 32.10 | 66.60 | 7.80 | 27.10 | 5.60 | 1.14 | 4.99 | 0.77 | 4.44 | 0.85 | 2.46 | 0.37 | 2.23 | 0.35 |
| 360-365 | 35.80 | 74.20 | 8.66 | 30.40 | 6.26 | 1.24 | 5.50 | 0.83 | 4.94 | 0.96 | 2.67 | 0.39 | 2.42 | 0.38 |
| 380-385 | 35.20 | 70.80 | 8.43 | 30.10 | 6.05 | 1.24 | 5.41 | 0.83 | 4.95 | 0.92 | 2.62 | 0.40 | 2.42 | 0.40 |
| 400-405 | 38.10 | 77.70 | 9.12 | 32.60 | 6.44 | 1.31 | 5.66 | 0.88 | 4.97 | 0.96 | 2.78 | 0.41 | 2.55 | 0.38 |
| 420-425 | 39.00 | 79.80 | 9.25 | 33.30 | 6.61 | 1.39 | 5.93 | 0.91 | 5.35 | 1.00 | 2.88 | 0.43 | 2.63 | 0.41 |
| 440-445 | 36.40 | 75.40 | 8.76 | 31.20 | 6.09 | 1.30 | 5.51 | 0.86 | 4.86 | 0.93 | 2.62 | 0.39 | 2.44 | 0.38 |
| 460-465 | 35.20 | 73.30 | 8.57 | 30.20 | 5.99 | 1.30 | 5.48 | 0.82 | 4.76 | 0.94 | 2.67 | 0.40 | 2.48 | 0.39 |
| 480-485 | 32.50 | 67.50 | 7.86 | 27.70 | 5.54 | 1.17 | 5.02 | 0.75 | 4.54 | 0.86 | 2.45 | 0.37 | 2.27 | 0.37 |
| 500-505 | 32.50 | 66.20 | 7.73 | 28.20 | 5.61 | 1.17 | 4.90 | 0.73 | 4.47 | 0.84 | 2.45 | 0.36 | 2.26 | 0.35 |
| 520-525 | 35.90 | 75.00 | 8.65 | 31.20 | 6.20 | 1.27 | 5.39 | 0.82 | 4.82 | 0.91 | 2.61 | 0.38 | 2.39 | 0.37 |
| 540-545 | 35.00 | 72.80 | 8.49 | 29.90 | 6.09 | 1.22 | 5.33 | 0.81 | 4.80 | 0.90 | 2.52 | 0.38 | 2.35 | 0.39 |
| 560-565 | 31.80 | 65.90 | 7.72 | 27.00 | 5.45 | 1.17 | 4.98 | 0.77 | 4.41 | 0.84 | 2.49 | 0.36 | 2.22 | 0.36 |
| 580-585 | 35.10 | 71.50 | 8.37 | 30.40 | 6.02 | 1.24 | 5.24 | 0.81 | 4.73 | 0.91 | 2.55 | 0.38 | 2.38 | 0.40 |

(Figure 5). It indicates that there is no significant correlation between particle size and REEs, Sr-Nd isotopes, and the separation of sediments due to particle size during transportation has a small impact on the results. The sources of sediment are the most important determining factor for REEs and Sr-Nd isotopes.

## 5.2 Evidence of REEs

During the sedimentation of marginal seas, the factor that has the greatest influence on the REE composition of marine sediment is the source of marine sediment (Yang et al., 2002), which have also been demonstrated in previous Discussion 5.1. The REE characteristics of sediments inherit the geochemical characteristics of the sources. The composition and distribution pattern of REEs in sediment mainly depend on the composition of source rocks, and have little variation during weathering, river erosion and transportation, deposition, diagenesis and metamorphism (Huang et al., 2023). The characteristic parameters of REEs are of great significance for exploring the formation conditions and provenance analysis of sediment (Kimoto et al., 2006; Stevens and Quinton, 2008).

10.3389/fmars.2024.1462439

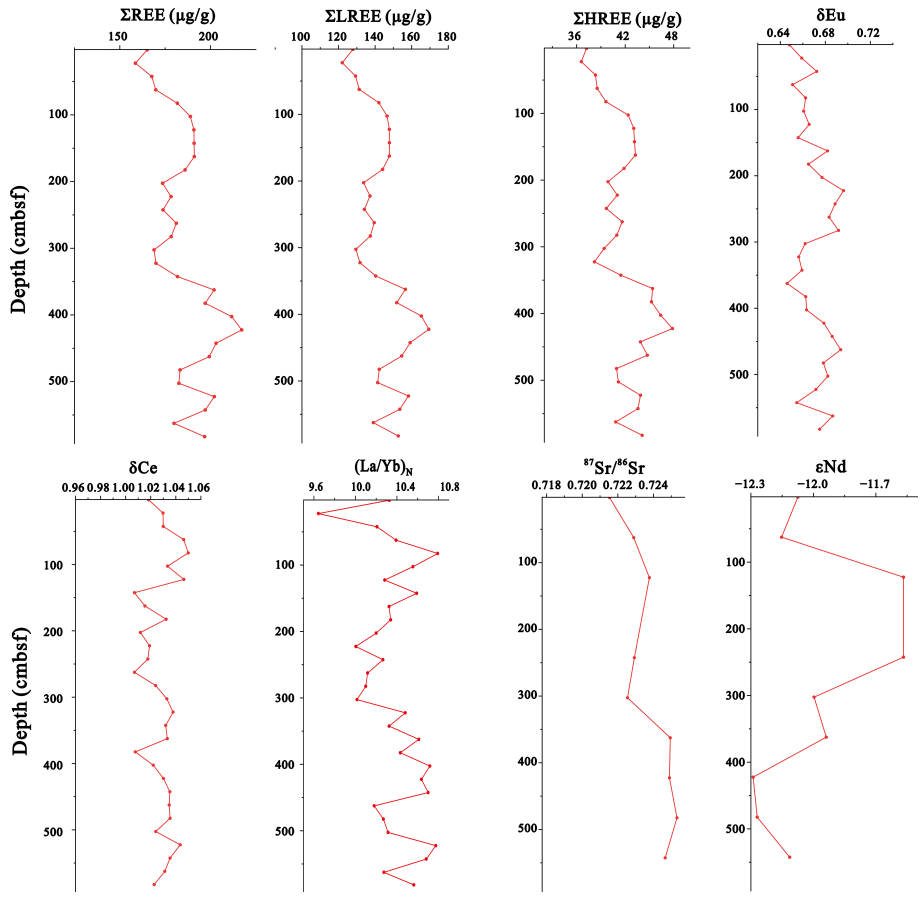


FIGURE 3
Variations of ΣREE, ΣLREE, ΣHREE, δEu, δCe, $(La/Yb)_N$, $^{87}Sr/^{86}Sr$, εNd at the core Z18.

The average ΣREE value of the samples is 160.5μg/g, which is close to the upper crust ΣREE (146.4μg/g) (Taylor and McLennan, 1981), much lower than the ΣREE of deep-sea clay(411 μg/g), but higher than the ΣREE of oceanic basalt (58.6 μg/g) (Frey and Haskin, 1964). The LREEs dominated in REEs, which shows that the sedimentation is mainly terrigenous contribution. As the increase of depth, ΣREE, ΣLREE, ΣHREE all shows a similar increasing trend.

TABLE 3 Comparison of the geochemical parameters of REE of Z18 site with surrounding areas (More data can be found in Appendix S2).

| Sample Area | ΣREEs | ΣLREE | ΣHREE | LREE/HREE | δCe | δEu | $(La/Yb)_N$ | $(La/Sm)_N$ | $(Gd/Yb)_N$ | Data Source |
|---|---|---|---|---|---|---|---|---|---|---|
| Z18 | 160.5133 | 143.7963 | 16.7170 | 8.5987 | 1.0283 | 0.6707 | 10.3710 | 3.7677 | 1.8310 | this article |
| The Pearl River | 91.0509 | 76.5284 | 14.5225 | 4.9716 | 0.6625 | 1.0316 | 7.2272 | 3.3713 | 1.9913 | (Xu and Han, 2009) |
| The Hainan Island | 123.1150 | 113.7300 | 9.3850 | 12.2800 | 1.1500 | 0.5950 | 13.2700 | 4.2750 | 1.6000 | (Wei et al., 2012) |
| The Taiwan River | 193.1224 | 173.6661 | 19.4563 | 8.8832 | 1.0282 | 0.6571 | 10.3953 | 4.2226 | 1.7818 | (Li et al., 2013) |
| Luzon | 73.1320 | 61.5920 | 11.5400 | 5.2180 | 0.9730 | 1.0540 | 5.1310 | 2.5890 | 1.4560 | (Tam et al., 2005) |
| Banda Sunda Arc | 136.2033 | 108.4833 | 27.7200 | 3.8978 | 0.9456 | 0.7956 | 3.2389 | 1.7689 | 1.4611 | (Handley et al., 2008) |
| Beibuwan | 126.3550 | 115.2867 | 11.0683 | 10.3367 | 1.1833 | 0.6167 | 10.0950 | 4.1567 | 1.3683 | (Wei et al., 2012) |
| Borneo | 142.9640 | 129.1420 | 13.8220 | 9.1600 | 1.4860 | 0.5860 | 7.7700 | 4.0080 | 1.1980 | (Wei et al., 2012) |
| The Philippines | 80.9867 | 71.2650 | 9.7217 | 7.4200 | 1.3367 | 0.6883 | 6.6700 | 3.6817 | 1.2600 | (Wei et al., 2012) |
| The Red River | 174.1674 | 158.2039 | 15.9635 | 9.6370 | 0.9926 | 0.6343 | 11.5404 | 4.7104 | 1.4957 | (Borges et al., 2008) |
| Mekong River | 193.2093 | 172.7207 | 20.4886 | 8.2421 | 0.9950 | 0.5671 | 9.4986 | 4.1043 | 1.6129 | (Borges et al., 2008) |

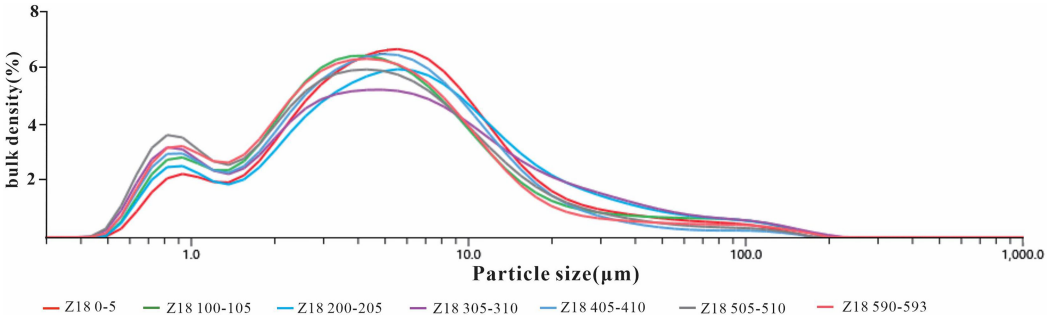


FIGURE 4
Particle size distribution curves of sediment at different depths in Z18 site.

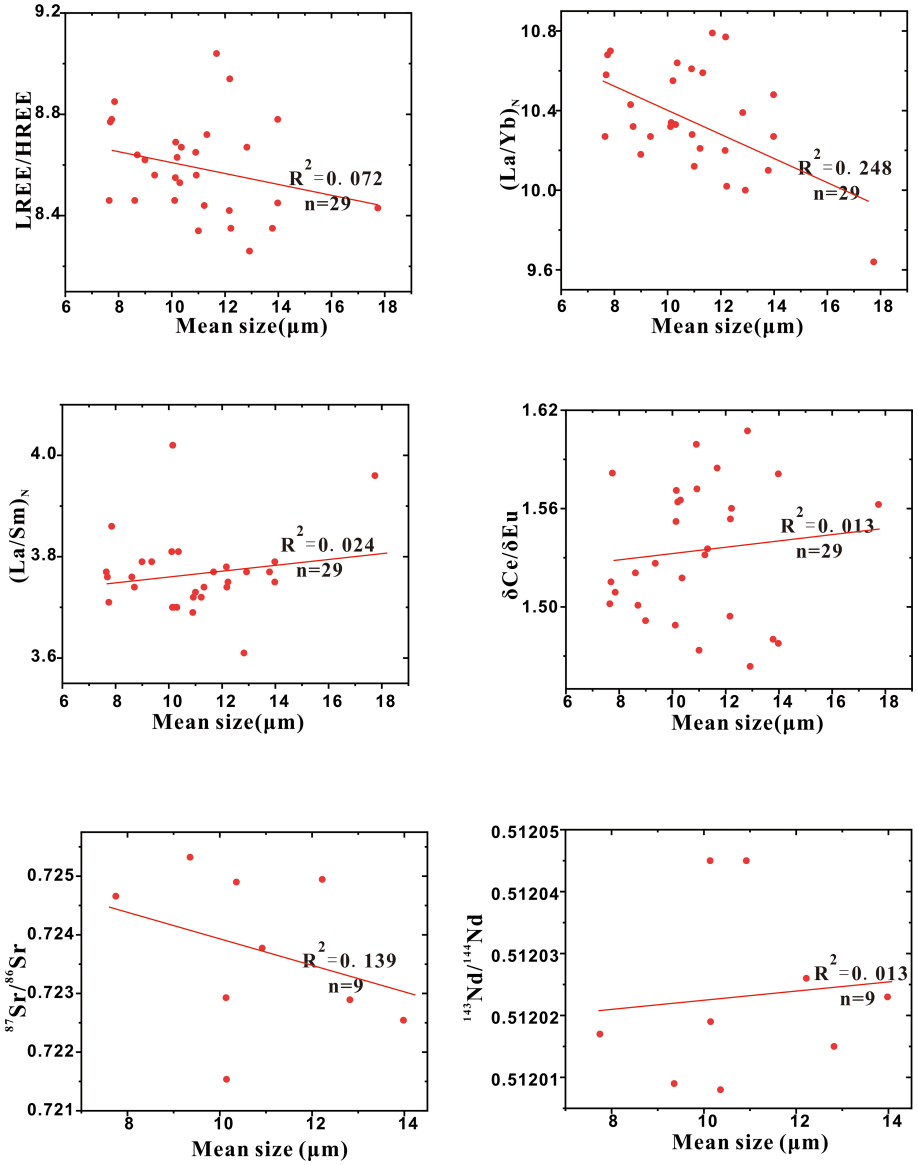


FIGURE 5
Correlation plots of mean size with REE and Sr-Nd isotope parameters including LREE/HREE, $(La/Yb)_N$, $(La/Sm)_N$, δCe/δEu, $^{87}Sr/^{86}Sr$ and $^{143}Nd/^{144}Nd$.

In order to further identify and compare the characteristics of different sources, the REEs of samples are standardized using oceanic basalt (Sun and McDonough, 1989) and compared with the chondrite-normalized distribution model of the Pearl River, Hainan Island, Taiwan Island, Luzon, Banda Sunda arc, the Beibu Gulf, Borneo, Philippines, Red River and Mekong River (Table 3, more data can be found in Appendix S2). It can be seen from the Figure 6 that the REE characteristic parameters of river sediment from different sources have significant differences, which can be used as evidences for source identification. The chondrite-normalized distribution model of the samples reflects the depletion of Eu (Figure 6, Table 3; Supplementary Table S2), a moderate degree enrichment of Gd (Figure 6), indicating oxygen rich environment in the sediment source area. Therefore, there is a steep pattern change of LREE while the pattern change of HREE is gentle. Compared with chondrite-normalized distribution model of sediment from different sources, it can be clearly found that the characteristics of our samples are closest to that of the Red River, followed by Taiwan Island, Hainan Island, and the Beibu Gulf. The chondrite-normalized distribution model of REEs of Mekong sediment is rather close to the sample, except for the greater depletion of Eu. The REE composition curves of sediment from Sunda arc, Borneo and the Philippines are significantly different from Z18 site. It shows that the Red River, Taiwan Island, Hainan Island, and Mekong River are potential sources of the Zhongjiannan Basin (Figure 6).

Previous studies have showed that the δEu and δCe values reflect the degree of weathering of the source rock, which is of great significance for source tracing (Yang et al., 2002). In the process of weakly acidic weathering, $Ce^{4+}$ in rock is relatively easy to hydrolyze, precipitate and stay *in situ*, resulting in negative Ce abnormality. On the contrary, under strong alkaline conditions, $Ce^{4+}$ is susceptible to leaching separation and loss. In addition, the variation of δEu in the sedimentary system is determined by the composition of the source debris. During the weathering process, some chemical weathering can preferentially remove $Eu^{2+}$ (Cullers et al., 1975).

Therefore, the δEu of the sediment can also reflect the weathering characteristics of the sedimentary source zone. Combined with the δCe-δEu plot from different sources (Figure 7), it is obvious that the sediment data are more concentrated and located in overlapping positions of many areas, indicating that the source of the Zhongjiannan Basin is complex and mixed. In addition, the sample data are mostly located in Area I (Mekong River), Area II (Red River), Area III (Taiwan); Furthermore, the sample data have a shared area with Area V (Pearl River) and are adjacent to Area III (Hainan Island). During the process of strong chemical weathering, HREEs are more active than LREEs, so HREEEs are more likely to migrate in solution form, while LREEs tend to accumulate in weathering residues.

$(La/Yb)_N$ is the slope of the distribution curve in the standardized diagram of REE chondrites, reflecting the degree of inclination of the curve. Previous studies have shown that δEu-$(La/Yb)_N$ can be used as an effective method to distinguish sediments from different sources. This indicator has been successfully applied to the marginal seas of the Asian continent (Liu et al., 2019). Consistent with Figures 7 and 8, the sample data area of Z18 site is all located within the intersection area of Area I (Mekong River), Area II (Red River), and Area III (Taiwan) in the HREE/LREE diagram (Figure 9).

From this, we conclude that the main sources of sediments in deep water area of the Zhongjiannan Basin are the Mekong River, the Red River, and Taiwan. In addition, the Hainan Island and the Pearl River also have some contributions. But because Hainan Island has little sediment input to the South China Sea (about 0.5Mts./yr) (Yang et al., 2013), and the Pearl River is far away from Z18 site, so we suspect that Hainan Island and the Pearl River have less contribution to the sediments of the Zhongjiannan Basin.

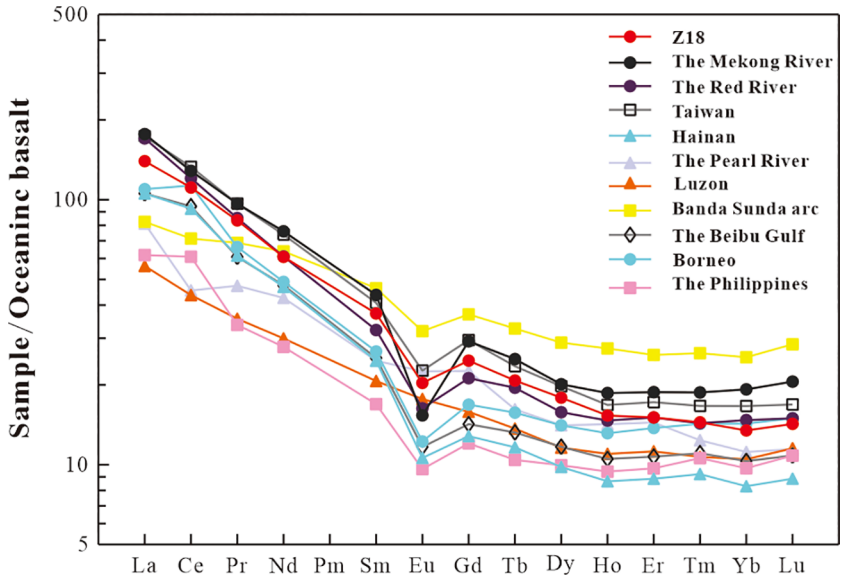


FIGURE 6
Chondrite-normalized distribution model of REEs in the core Z18 and different sources, the REE data are from Table 3. The REE data for chondrites were obtained from (Sun and McDonough, 1989).

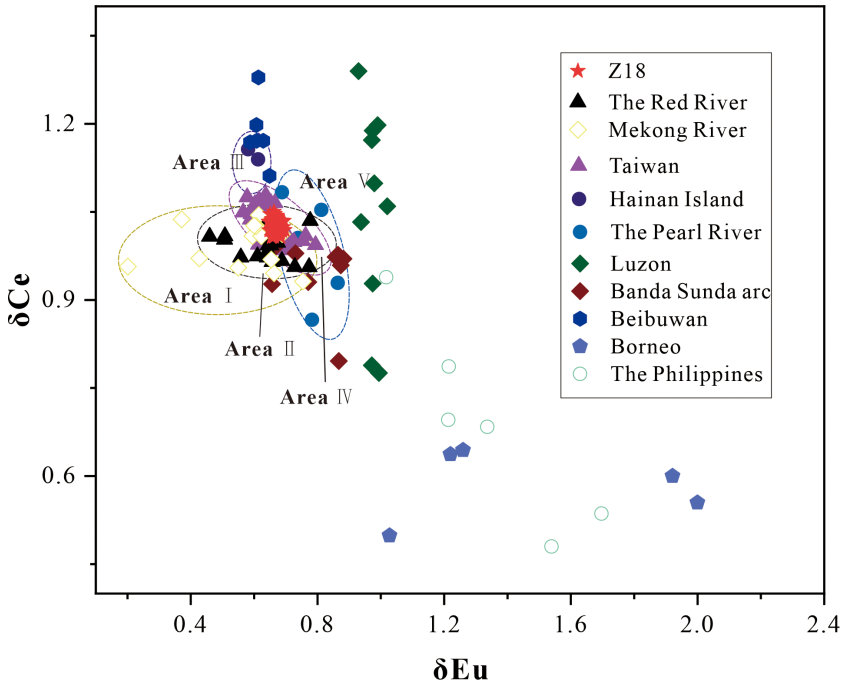


FIGURE 7
The correlation plots of δCe and δEu parameters in core Z18, Zhongjiannan Basin, the REE data are from Table 3. Area I: Mekong River; Area II: The Red River; Area III: Hainan Island; Area IV: Taiwan; Area V: The Pearl River.

## 5.3 Sr-Nd isotope analysis

Because the adjacent lands in the SCS have different degrees of weathering, the geochemistry of sediment from various rivers is diverse (Liu et al., 2016b). εNd is relatively stable during rock weathering, erosion, and river transport, thus it can be stable in the migration process (Steinke et al., 2003, 2006; Wei et al., 2012; Huang et al., 2016; Liu et al., 2017b). And many studies showed that εNd is unlikely affected by grain size. Goldstein et al., 1984 proposed the slight changes is only ±0.3 εNd in different size fractions in fluvial sediments. Moreover, there is a limited influence of grain size on εNd in aeolian sediments (Chen et al., 2007). Besides, the Sr isotopic compositions of rocks are determined by age and weathering degree. Therefore, the Sr-Nd isotopic composition of fluvial sediment is often used to trace their sources (Mahoney, 2005; Dou et al., 2012; Awasthi, 2017; Awasthi et al., 2018; Hu et al., 2018). As shown in the Figure 10, in order to further explore the provenance of surface sediments in the Zhongjiannan Basin, we collected published Sr-Nd isotopic data from river sediments of Hainan Island, Taiwan, Pearl River, Red River, Mekong River, Philippines, northern SCS slope, Luzon, Banda Sunda arc, Beibuwan, Borneo, and compared with our samples (More data can be found in Appendix S3). Sediments carried by rivers flowing through ancient crustal rocks have higher $^{87}Sr/^{86}Sr$ ratios and lower εNd value (<-6), while the sediments carried by rivers flowing through newly formed crustal rocks, it has a higher εNd value (> +5) and lower $^{87}Sr/^{86}Sr$ ratios (DePaolo and Johnson, 1979). Our samples are characterized by high $^{87}Sr/^{86}Sr$ ratios (average is 0.723722) and low εNd values (average is -11.9968), from which we can conclude that the provenance of the Zhongjiannan Basin is mainly ancient continental rocks. The Sr-Nd isotopes of the samples are relatively concentrated, and combined with particle size changes, indicating that the surface sediments in deep water area of the Zhongjiannan Basin are relatively stable. According to the correlation plots of $^{87}Sr/^{86}Sr$ with εNd parameters, we can clearly find that the sample data fall within the overlapping area of sediments from multiple regions, once again indicating that the sediment in the Zhongjiannan Basin are mixed sources. Among them, our sample data are completely covered by Area I (Red River). Secondly, the Z18 site data are relatively close to Area II (Mekong River), Area V (Taiwan), and Area III (southern shelf of Hainan), all of which have certain regional overlap. Our results are consistent with previous studies (Wei et al., 2012; Liu et al., 2016b). The Luzon archipelago is dominated by andesite-basalt volcanic sedimentary rocks (McDermott et al., 2005), with εNd values ranging from +6 to +8. In addition, εNd values of the Sunda arc range from +1 to +4, which is quite different from our sample data. According to Sr-Nd isotope data, we conclude that the Red River contributes significantly to the source of the Zhongjiannan Basin, the Mekong River, Taiwan and Hainan also have important contributions, and the sediment of the Pearl River also have a certain supply.

Previous studies have shown that the Red River (138Mts./yr) and Mekong River (166Mts./yr) transport a large amount of sediment to the SCS every year (Liu et al., 2016b). Meanwhile, we find that the REEs data and Sr-Nd isotopic data of the samples correspond best with the Red River and Mekong River. In addition, the Red River and Mekong River are relatively close to the Z18 site among all potential source areas, so we believe that the Red River and Mekong River are the largest sources of sediment in deep water area of the Zhongjiannan Basin, followed by Taiwan. Hainan Island and the Pearl River which also have small contributions.

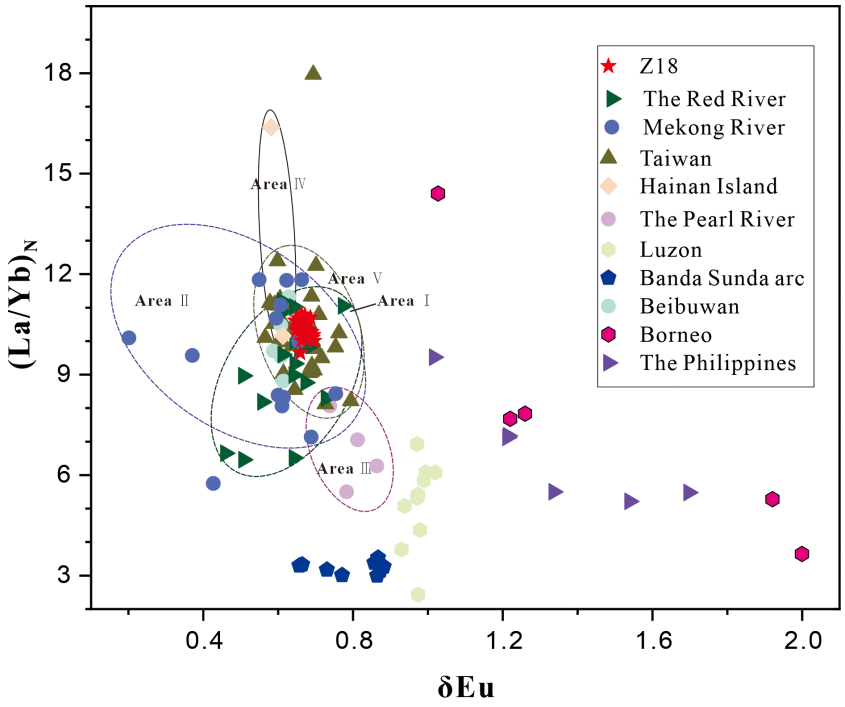


FIGURE 8
The correlation plots of $(La/Yb)_N$ and δEu parameters in core Z18, Zhongjiannan Basin, the REE data are from Table 3. Area I: The Red River; Area II: Mekong River; Area III: The Pearl River; Area IV: Hainan Island; Area V: Taiwan.

## 5.4 Transport mechanism

Marine sedimentation is mainly influenced by sources and transport processes (Zhao et al., 2015). It may also be related to changes in sedimentary environment, changes in sea level, coastline, and rivers, as well as the transformation process of early sediment (Liu et al., 2017a). Topography, migration distance, and annual suspended sediment discharge of fluvial drainage systems all have impacts on sediment transport. The main influencing factors on the transport of sediment in the SCS include coastal and surface currents controlled by the East Asian monsoon, Kuroshio (Liang et al., 2003), and deep current (Figure 11) (Liu et al., 2016a; Liu et al., 2016b).

Since the Pliocene, due to the increase of sediment in the Mekong River and changes in high sea levels, the sedimentary center of the SCS

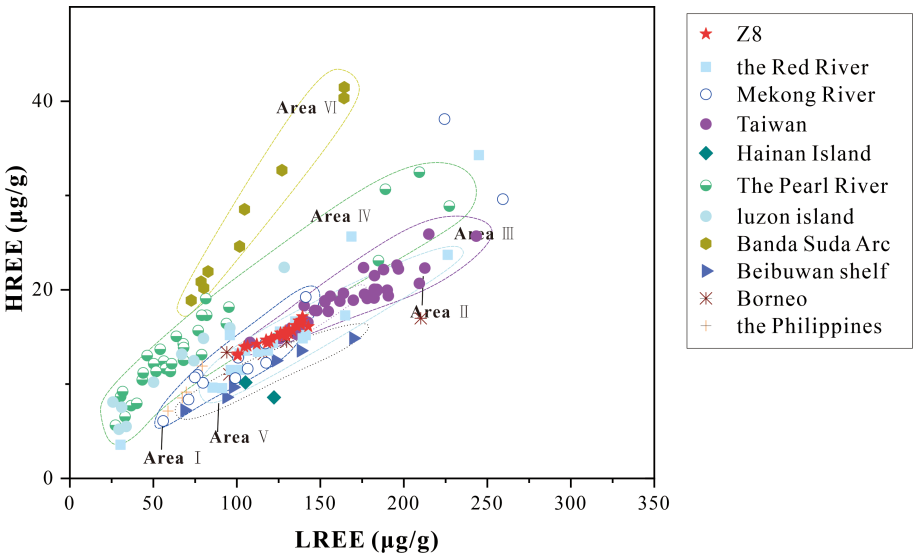


FIGURE 9
The correlation plots of HREE and LREE parameters in core Z18, Zhongjiannan Basin, the REE data are from Table 3. Area I: Mekong River; Area II: The Red River; Area III: Taiwan; Area IV: The Pearl River; Area V: Banda Suda Arc.

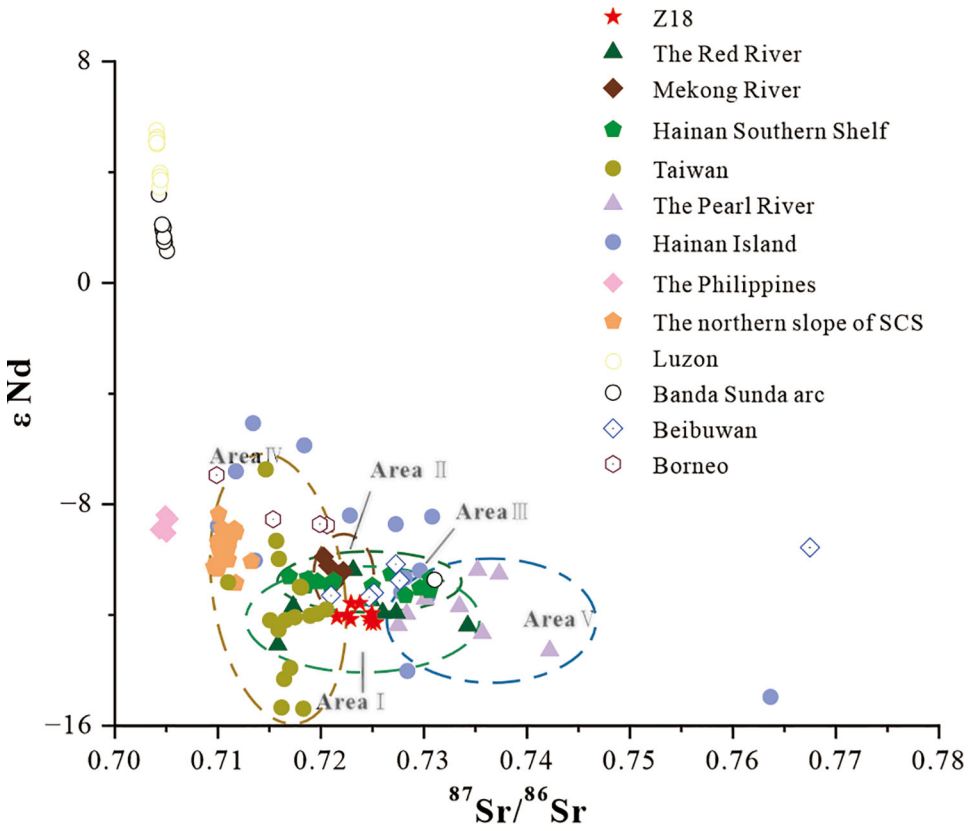


FIGURE 10
The correlation plots of $^{87}Sr/^{86}Sr$ and εNd parameters in core Z18 and surrounding fluvial drainage systems, the Sr, Nd isotope data are from Table 4 (More data can be found in Appendix S3). Area I: The Red River; Area II: Mekong River; Area III: Hainan Southern Shelf; Area IV: Taiwan; Area V: The Pearl River.

has gradually shifted from the northern to the southern (Wang and Ding, 2023). The surface current of the SCS is controlled by the monsoon system. Because of the influence of the monsoon, the speed and direction of surface current in the SCS vary seasonally. In winter, surface current flows southwestward driven by the northeast monsoon, while in summer, surface current flows driven northeast by the southwest monsoon (Fang et al., 1998). In summer, driven by the southwest monsoon, surface current transports sediment carried by the Mekong River towards the northeast, which is also the main transportation route for sediment from the Mekong River to the Zhongjiannan Basin (Figure 11). Previous studies also indicated that the sediments of the Mekong River mainly move through the surface current of the SCS to the western part of the South China Sea for hundreds of kilometers (Cai et al., 2022). In addition, Liu et al., 2016b have used clay minerals to demonstrate the influence of the western ocean current in the SCS on sediment transport. Due to the influence of the monsoon and changes in ocean currents, illite and chlorite from the Mekong River are transported northward (Liu et al., 2016b). The sediments carried by the Mekong River and central Vietnamese rivers are difficult to reach the northern shelf and slope areas of the South China Sea (Liu et al., 2010b), so most of the sediment is deposited in the central and southern of SCS. In winter, when the monsoon driver surface current southwest, surface current carries sediment from the Red River which has been driven to the northern slope of the SCS to the central part of the SCS. This also carries a certain amount of sediment of Hainan Island. Studies have proposed that the sediment of the Red River can be transported to the western SCS through the southern channel, making it an important source of sediment in the Xisha Trough (Wan et al., 2015; Li et al., 2019), which is consistent with our results. Although the sediment flux of Hainan Island is much smaller than that of the Red River, the contribution of Hainan Island to the inland shelf sediment is an essential factor (Cai et al., 2020). At the same time, the sediment in the SCS is also affected by coastal currents, mainly including the Guangdong Coastal Current (GDCC) and the Northwest Luzon Coastal Current. In winter, GDCC moves southward and southwestward along the continental margin, carrying the sediment of the Red River and the Pearl River. However, due to the weak coastal flow force and low speed, the sediment of the Red River is migration nearby and easily settled down. Previous studies also have showed that the sediment carried by the Red River is almost deposited in the Beibu Gulf Basin, Qiongdongnan Basin, Yinggehai Basin and transports southward due to the blocking of Hainan Island (Liu et al., 2010a), while the surface current driven by the monsoon in winter will continue to transport the settled sediment southward, to reach the center of the SCS.

The cyclone circulation in the deep basins of the SCS is mainly caused by deep water circulation (Wang et al., 2011). The deep-sea current from the Pacific enters the SCS through the Luzon Strait,

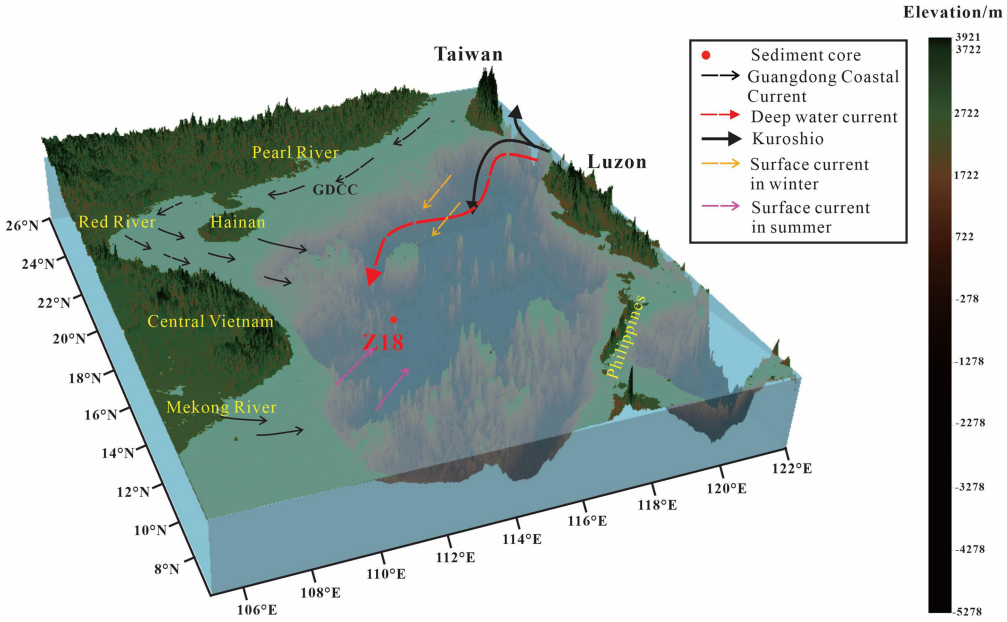


FIGURE 11
3-D topographic map showing the transport pattern of the Zhongjiannan Basin (modified from (Liu et al., 2016b; Cai et al., 2020; Geng et al., 2020; Cai et al., 2022; Huang et al., 2023).

TABLE 4 Sr-Nd isotopes of the sediment of Z18 and different sources area.

| No | Sample | Depth (cmbsf) | $^{87}Sr/^{86}Sr$ | 2ð | $^{143}Nd/^{144}Nd$ | 2ð | εNd | Data source |
|---|---|---|---|---|---|---|---|---|
| 1 | Z18 | 0-5 | 0.721537 | 0.000010 | 0.512019 | 0.000003 | -12.074797 | This Study |
| 2 | Z18 | 60-65 | 0.722893 | 0.000005 | 0.512015 | 0.000003 | -12.152825 | This Study |
| 3 | Z18 | 120-125 | 0.723774 | 0.000004 | 0.512045 | 0.000004 | -11.567617 | This Study |
| 4 | Z18 | 180-185 | 0.722928 | 0.000005 | 0.512045 | 0.000004 | -11.567617 | This Study |
| 5 | Z18 | 240-245 | 0.722544 | 0.000004 | 0.512023 | 0.000002 | -11.996770 | This Study |
| 6 | Z18 | 300-305 | 0.724945 | 0.000004 | 0.512026 | 0.000003 | -11.938249 | This Study |
| 7 | Z18 | 420-425 | 0.724899 | 0.000005 | 0.512008 | 0.000003 | -12.289374 | This Study |
| 8 | Z18 | 480-485 | 0.725322 | 0.000006 | 0.512009 | 0.000002 | -12.269867 | This Study |
| 9 | Z18 | 520-525 | 0.724658 | 0.000005 | 0.512017 | 0.000003 | -12.113811 | This Study |
| 10 | Hainan Island (Average value) | – | 0.725435 | – | 0.512145 | – | -9.618316 | (Lei et al., 2022) |
| 11 | Taiwan River (Average value) | – | 0.716789 | – | 0.512027 | – | -11.923332 | (Chen et al., 1990) |
| 12 | The Pearl River (Average value) | – | 0.733727 | – | 0.512034 | – | -11.782193 | (Liu et al., 2007) |
| 13 | The Red River (Average value) | – | 0.724090 | – | 0.512031 | – | -11.832354 | (Liu et al., 2007) |
| 14 | The Mekong River (Average value) | – | 0.721251 | – | 0.512106 | – | -10.377693 | (Liu et al., 2007) |
| 15 | The Philippines (Average value) | – | 0.704880 | – | 0.512191 | – | -8.714727 | (Goldstein and Jacobsen, 1988) |
| 16 | The northern slope of SCS (Average value) | – | 0.710700 | – | 0.512146 | – | -9.589830 | (Cai et al., 2020) |
| 17 | Luzon (Average value) | – | 0.704360 | – | 0.512875 | – | 4.624539 | (DuFrane et al., 2006) |

*(Continued)*

TABLE 4 Continued

| No | Sample | Depth (cmbsf) | $^{87}Sr/^{86}Sr$ | 2ð | $^{143}Nd/^{144}Nd$ | 2ð | εNd | Data source |
|---|---|---|---|---|---|---|---|---|
| 18 | Hainan Southern Shelf (Average value) | – | 0.724200 | – | 0.512078 | – | -10.925513 | (Cai et al., 2020) |
| 19 | Banda Sunda arc (Average value) | – | 0.707347 | – | 0.512670 | – | 0.618370 | (Handley et al., 2008) |
| 20 | Beibuwan (Average value) | – | 0.732905 | – | 0.512100 | – | -10.497986 | (Wei et al., 2012) |
| 21 | Borneo (Average value) | – | 0.716439 | – | 0.512216 | – | -8.241683 | (Wei et al., 2012) |

and moves northwest, then turns southwest along the continental margin (Qu et al., 2006). Observation has found that deep water current bifurcates into two tributaries after entering the Zhongsha Islands (Figure 11), and one branch forms the cyclonic circulation around the deep basin and seamount in the central SCS; another flow continuously along the 3500m isobath (Qu et al., 2006; Wang et al., 2018). The unique topography, high precipitation, and active tectonic environment of Taiwan Island produce a large amount of sediment (Liu et al., 2008), which is directly transported to the central SCS through deep water current (Syvitski, 2003). Taiwan-derived sediments can be transported southwest to a depth of 2500m by deep-water circulation (Liu et al., 2011).

Huang et al., 2023 proposed that the movement of subsurface waters in the SCS may be related to the Kuroshio (Huang et al., 2023). Kuroshio is a branch of the North Equatorial Warm Current deflecting to the north, one of the important warm currents of the Northwest Pacific Subtropical Circulation. After entering the SCS, under the influence of factors such as topography and wind, the SCS branch is formed in southwest Taiwan (Hsueh, 2000). Although the Kuroshio does not directly affect deep seawater, it has an undeniable impact on the flow of deep seawater. The Kuroshio transports a portion of sediments near Taiwan towards the southwest to the eastern of the SCS, and then the surface circulation and deep circulation of the SCS further move the sediment southward to the central part of the SCS.

## 6 Conclusion

In this study, we analyzed the grain size characteristics, REEs, and Sr-Nd isotopes of gravity core sediments in deep water area of the Zhongjiannan Basin, and explored its provenance and transportation mechanisms. The main conclusions are as follows:

1. Based on the particle size characteristics, we found that the sedimentation in the Zhongjiannan Basin is stable and relatively continuous, with no significant changes in the source within a certain time scale. Combining particle size with REEs and Sr-Nd isotope characteristics, we found that the REEs and Sr-Nd isotope characteristics of sediments are not significantly related to particle size, indicating that the geochemical characteristics of sediments largely depend on sediment sources.
2. The average ΣREE content is 160.5μg/g and the LREEs dominated in REEs, which shows that the sediment is mainly terrigenous source. The sediment sources in deep water area of the Zhongjian South Basin mainly include (1) the Red River; (2) the Mekong River; (3) Taiwan; (4) Hainan Island; (5) the Pearl River. The abundant input of terrestrial sediment from the Red River and the Mekong River have made the largest source of the Zhongjiannan Basin. Taiwan also has a significant source of sediment contribution. Hainan Island and the Pearl River also transport small amount of sediment to the Zhongjiannan Basin.
3. Topography, migration distance, and annual suspended sediment discharge of fluvial drainage systems all have impacts on sediment transport. The surface current from southwest to northeast in winter causes substantial sediment to migrate from the Mekong River to the Zhongjiannan Basin; the surface current from northeast to southwest in summer and the deep water current make Taiwan a significant source contribution to the Zhongjiannan Basin; the surface current from northeast to southwest in summer and GDCC transport sediment from the Red River and Hainan Island to Z18 site; the Kuroshio also contributes to the migration of sediment in Taiwan.

## Data availability statement

The original contributions presented in the study are included in the article/Supplementary Material. Further inquiries can be directed to the corresponding author.

## Author contributions

XW: Software, Methodology, Investigation, Writing – review & editing, Writing – original draft. CS: Software, Methodology, Investigation, Data curation, Writing – original draft. FG: Writing – original draft, Methodology, Data curation, Conceptualization. ZL: Writing – original draft, Validation, Project administration, Data curation. JL: Writing – original draft, Supervision, Project administration, Formal Analysis. PL: Writing – original draft, Project administration, Formal Analysis. ZWang: Writing – original draft,

Validation, Resources, Funding acquisition. GW: Writing – original draft, Visualization, Supervision. ZWan: Validation, Supervision, Resources, Methodology, Conceptualization, Writing – review & editing, Writing – original draft.

## Funding

The author(s) declare that financial support was received for the research, authorship, and/or publication of this article. This research was supported by the National Nature Science Foundation of China (No. 42076054), Key R&D projects in Hainan Province (No. ZDYF2023GXJS008).

## Acknowledgments

Thanks are due to the Southern Marine Science and Engineering Guangdong Laboratory (Zhuhai) for samples testing. We also thank the National Natural Science Foundation of China Shared Voyage Program "Experimental Study on the 2021 Central South China Sea Basin Scientific Survey of the Shared Voyage Plan", which offered the study samples.

## Conflict of interest

The authors declare that the research was conducted in the absence of any commercial or financial relationships that could be construed as a potential conflict of interest.

## Publisher's note



## Supplementary material

The Supplementary Material for this article can be found online at: https://www.frontiersin.org/articles/10.3389/fmars.2024.1462439/full#supplementary-material

SUPPLEMENTARY FIGURE 1
XRD results of the studied sediment cores.

## References

Awasthi, N. (2017). Provenance and paleo-weathering of Tertiary accretionary prism-forearc sedimentary deposits of the Andaman Archipelago, India. *J. Asian Earth Sci.* 150, 45–62. doi: 10.1016/j.jseaes.2017.10.005

Awasthi, N., Ray, E., and Paul, D. (2018). Sr and Nd isotope compositions of alluvial sediments from the Ganga Basin and their use as potential proxies for source identification and apportionment. *Chem. Geol.* 476, 327–339. doi: 10.1016/j.chemgeo.2017.11.029

Borges, J. B., Huh, Y., Moon, S., and Noh, H. (2008). Provenance and weathering control on river bed sediments of the eastern Tibetan Plateau and the Russian Far East. *Chem. Geol.* 254, 52–72. doi: 10.1016/j.chemgeo.2008.06.002

Cai, G., Li, S., Zhao, L., Zhong, L., and Chen, H. (2020). Clay minerals, Sr-Nd isotopes and provenance of sediments in the northwestern South China Sea. *J. Asian Earth Sci.* 202. doi: 10.1016/j.jseaes.2020.104531

Cai, G., Xu, Y., Zhong, H., and Cheng, Y. (2022). Terrigenous and volcanogenic contribution to the deep basin of the South China Sea: Evidence from trace elements and Sr-Nd isotopes. *Mar. Geol.* 448. doi: 10.1016/j.margeo.2022.106811

Chen, C. H., Jahn, B., Lee, T., Chen, C., and Cornichet, J. (1990). Sm-Nd isotopic geochemistry of sediments from Taiwan and implications for the tectonic evolution of southeast China. *Chem. Geol.* 88, 317–332. doi: 10.1016/0009-2541(90)90096-p

Chen, J., Li, G., Yang, J., Rao, W., Lu, H., Balsam, W., et al. (2007). Nd and Sr isotopic characteristics of Chinese deserts: Implications for the provenances of Asian dust. *Geochim. Cosmochim. Acta* 71, 3904–3914. doi: 10.1016/j.gca.2007.04.033

Chen, M., Wang, R., Yang, L., Han, J., and Lu, J. (2003). Development of east Asian summer monsoon environments in the late Miocene: radiolarian evidence from Site 1143 of ODP Leg 184. *Mar. Geol.* 201, 169–177. doi: 10.1016/S0025-3227(03)00215-9

Clift, P. D., Wan, S., and Blusztajn, J. (2014). Reconstructing chemical weathering, physical erosion and monsoon intensity since 25 Ma in the northern South China Sea: A review of competing proxies. *Earth-Sci. Rev.* 130, 86–102. doi: 10.1016/j.earscirev.2014.01.002

Cullers, R., Chaudhuri, S., Lee, B. A. M., and Wolf, C. (1975). Rare earth distributions in clay minerals and in the clay-sized fraction of the Lower Permian Havensville and Eskridge shales of Kansas and Oklahoma. *Geochim. Cosmochim. Acta* 12, 1691–1703. doi: 10.1016/0016-7037(75)90090-3

Deng, F., Hellmann, S., Zimmermann, T., and Proefrock, D. (2021). Using Sr-Nd-Pb isotope systems to trace sources of sediment and trace metals to the Weser River system (Germany) and assessment of input to the North Sea. *Sci. Total Environ.* 791. doi: 10.1016/j.scitotenv.2021.148127

DePaolo, D. J., and Johnson, R. W. (1979). Magma genesis in the New Britain island-arc; constraints from Nd and Sr isotopes and trace-element patterns. *Contrib. Mineral. Petrol.* 70, 367–379. doi: 10.1007/BF00371044

Dimitrov, L. I. (2002). Mud volcanoes; the most important pathway for degassing deeply buried sediments. *Earth-Sci. Rev.* 59, 49–76. doi: 10.1016/S0012-8252(02)00069-7

Dou, Y., Yang, S., Liu, Z., Shi, X., Li, J., Yu, H., et al. (2012). Sr-Nd isotopic constraints on terrigenous sediment provenances and Kuroshio Current variability in the Okinawa Trough during the late Quaternary. *Palaeogeogr. Palaeoclimatol. Palaeoecol.* 365, 38–47. doi: 10.1016/j.palaeo.2012.09.003

DuFrane, S. A., Asmerom, Y., Mukasa, S. B., Morris, J. D., and Dreyer, B. M. (2006). Subduction and melting processes inferred from U-Series Sr - Nd - Pb isotope, and trace element data, Bicol and Bataan arcs, Philippines. *Geochim. Cosmochim. Acta* 70, 3401–3420. doi: 10.1016/j.gca.2006.04.020

Fang, G., Fang, W., Fang, Y., and Wang, K. (1998). A survey of studies on the South China Sea upper ocean circulation. *Acta Oceanographica Taiwanica.* 37, 1–16.

Feng, X., Wu, Y. H., Yang, B. J., Shan, X., and Liu, J. H. (2021). Records of Hyperpycnal Flow Deposits in the Southwestern Okinawa Trough and Their Paleoclimatic Response since 1.3 ka. *Acta Sedimentologica Sinica.* 39, 739–750. doi: 10.14027/j.issn.1000-0550.2020.018

Frey, F., and Haskin, L. (1964). Rare earths in oceanic basalts. *J. Geophysical Reasearch.* 4, 775-780. doi: 10.1029/JZ069i004p00775

Fyhn, M. B., Boldreel, L. O., and Nielsen, L. H. (2009). Geological development of the Central and South Vietnamese margin: Implications for the establishment of the South China Sea, Indochinese escape tectonics and Cenozoic volcanism. *Tectonophysics.* 478, 184–214. doi: 10.1016/j.tecto.2009.08.002

Geng, M., Song, H., Guan, Y., Chen, J., Zhang, R., Zhang, B., et al. (2020). Sill-related seafloor domes in the Zhongjiannan Basin, western South China Sea. *Mar. Pet. Geol.* 122. doi: 10.1016/j.marpetgeo.2020.104669

Goldstein, S. J., and Jacobsen, S. B. (1988). Nd and Sr isotopic systematics of river water suspended material; implications for crustal evolution. *Earth Planet. Sci. Lett.* 87, 249–265. doi: 10.1016/0012-821X(88)90013-1

Goldstein, S. L., Nions, R. K., and Hamilton, P. J. (1984). A Sm-Nd isotopic study of atmospheric dusts and particulates from major river systems. *Earth Planet. SC. Lett.* 70, 221–236. doi: 10.1016/0012-821x(84)90007-4

Gong, Y., Pease, V., Wang, H., Gan, H., Liu, E., Ma, Q., et al. (2021). Insights into evolution of a rift basin: Provenance of the middle Eocene-lower Oligocene strata of the Beibuwan Basin, South China Sea from detrital zircon. *Sediment. Geol.* 419. doi: 10.1016/j.sedgeo.2021.105908

Handley, H. K., Davidson, J. P., Macpherson, C. G., and Stimac, J. A. (2008). Untangling differentiation in arc lavas: Constraints from unusual minor and trace element variations at Salak Volcano, Indonesia. *Chem. Geol.* 255, 360–376. doi: 10.1016/j.chemgeo.2008.07.007

Hsueh, Y. (2000). The kuroshio in the east China sea. *J. Mar. Syst.* 24, 131–139. doi: 10.1016/S0924-7963(99)00083-4

Hu, B., Li, J., Zhao, J., Yan, H., Zou, L., Bai, F., et al. (2018). Sr-Nd isotopic geochemistry of Holocene sediments from the South Yellow Sea: Implications for provenance and monsoon variability. *Chem. Geol.* 479, 102–112. doi: 10.1016/j.chemgeo.2017.12.033

Hu, Z., Huang, B., Geng, L., and Wang, N. (2022). Sediment provenance in the Northern South China Sea since the Late Miocene. *Open Geosci.* 14, 1636–1649. doi: 10.1515/geo-2022-0454

Huang, J., Wan, S., Xiong, Z., Zhao, D., Liu, X., Li, A., et al. (2016). Geochemical records of Taiwan-sourced sediments in the South China Sea linked to Holocene climate changes. *Palaeogeogr. Palaeoclimatol. Palaeoecol.* 441, 871–881. doi: 10.1016/j.palaeo.2015.10.036

Huang, Q., Hua, Y., Zhang, C., Cheng, P., Wan, Z., Hong, T., et al. (2023). Provenance and transport mechanism of gravity core sediments in the deep-water area of the Qiongdongnan Basin, northern South China Sea. *Mar. Geol.* 459. doi: 10.1016/j.margeo.2023.107043

Jacobsen, S., and Wasserburg, G. (1980). Sm-Nd isotopic evolution of chondrites Earth Planet. *SC. Lett.* 50), 139–155. doi: 10.1016/0012-821X(80)90125-9

Jaijel, R., Goodman Tchernov, B. N., Biton, E., Weinstein, Y., and Katz, T. (2021). Optimizing a standard preparation procedure for grain size analysis of marine sediments by laser diffraction (MS-PT4SD: Marine sediments-pretreatment for size distribution). *Deep Sea Res. Part I: Oceanographic Res. Papers.* 167, 103429. doi: 10.1016/j.dsr.2020.103429

Kimoto, A., Nearing, M. A., Zhang, X. C., and Powell, D. M. (2006). Applicability of rare earth element oxides as a sediment tracer for coarse-textured soils. *Catena.* 65, 214–221. doi: 10.1016/j.catena.2005.10.002

Kuehl, S., and Nittrouer, C. (2011). Exploring the transfer of earth suface materials from source to sink. *Geophys* 92, 188–188. doi: 10.1029/2011EO220007

Lei, Z., Fahai, M., Chaoqun, W., Liyun, J., Yaoling, Z., Dongxia, S., et al. (2022). Sr-Nd Isotopic Composition and provenance of Late Cenozoic Sediments in northern Hainan Island. *Geological Bullrtin China.* 41, 1996–2006.

Li, C., Shi, X., Kao, S., Liu, Y., Lyu, H., Zou, J., et al. (2013). Rare earth elements in fine-grained sediments of major rivers from the high-standing island of Taiwan. *J. Asian Earth Sci.* 69, 39–47. doi: 10.1016/j.jseaes.2013.03.001

Li, M., Ouyang, T., Zhu, Z., Tian, C., Peng, S., Tang, Z., et al. (2019). Rare earth element fractionations of the northwestern South China Sea sediments, and their implications for East Asian monsoon reconstruction during the last 36 kyr. *Quat. Int.* 525, 16–24. doi: 10.1016/j.quaint.2019.09.007

Li, S., Lin, C., Zhang, Q., Yang, S., and Wu, P. (1999). Episodic rifting of continental marginal basins and tectonic events since 10 Ma in the South China Sea. *Chin. Sci. Bull.* 44, 10–22. doi: 10.1007/BF03182877

Liang, W. D., Tang, T. Y., Yang, Y. J., Ko, M. T., and Chuang, W. S. (2003). Upper-ocean currents around Taiwan. *Deep-Sea Res. Part II-Top. Stud. Oceanogr.* 50, 1085–1105. doi: 10.1016/S0967-0645(03)00011-0

Lim, D. I., Jung, H. S., Choi, J. Y., Yang, S., and Ahn, K. S. (2006). Geochemical compositions of river and shelf sediments in the Yellow Sea: Grain-size normalization and sediment provenance. *Cont. Shelf Res.* 26, 15–24. doi: 10.1016/j.csr.2005.10.001

Liu, C., Clift, P. D., Carter, A., Boening, P., Hu, Z., Sun, Z., et al. (2017a). Controls on modern erosion and the development of the Pearl River drainage fa in the late Paleogene. *Mar. Geol.* 394, 52–68. doi: 10.1016/j.margeo.2017.07.011

Liu, J., Steinke, S., Vogt, C., Mohtadi, M., De Pol-Holz, R., and Hebbeln, D. (2017b). Temporal and spatial patterns of sediment deposition in the northern South China Sea over the last 50,000 years. *Palaeogeogr. Palaeoclimatol. Palaeoecol.* 465, 212–224. doi: 10.1016/j.palaeo.2016.10.033

Liu, J., Xiang, R., Chen, M., Chen, Z., Yan, W., and Liu, F. (2011). Influence of the Kuroshio current intrusion on depositional environment in the Northern South China Sea: Evidence from surface sediment records. *Mar. Geol.* 285, 59–68. doi: 10.1016/j.margeo.2011.05.010

Liu, J., Xiang, R., Kao, S. J., Fu, S., and Zhou, L. (2016a). Sedimentary responses to sea - level rise and Kuroshio Current intrusion since the Last Glacial Maximum: Grain size and clay mineral evidence from the northern South China Sea slope. *Palaeogeogr. Palaeoclimatol. Palaeoecol.* 450, 111–121. doi: 10.1016/j.palaeo.2016.03.002

Liu, S., Zhang, H., Zhu, A., Wang, K., Chen, M., Khokiattiwong, S., et al. (2019). Distribution of rare earth elements in surface sediments of the western Gulf of Thailand: Constraints from sedimentology and mineralogy. *Quat. Int.* 527, 52–63. doi: 10.1016/j.quaint.2018.08.010

Liu, X., Wei, G., Zou, J., Guo, Y., Ma, J., Chen, X., et al. (2018). Elemental and sr-nd isotope geochemistry of sinking particles in the northern south China sea: implications for provenance and transportation. *J. Geophysical Research: Oceans.* 123, 9137–9155. doi: 10.1029/2018JC014312

Liu, Z., Colin, C., Huang, W., Chen, Z., Trentesaux, A., and Chen, J. F. (2007). Clay minerals in surface sediments of the Pearl River drainage basin and their contribution to the South China Sea. *Chin. Sci. Bulletin.* 52, 1101–1111. doi: 10.1007/s11434-007-0161-9

Liu, Z., Tuo, S., Colin, C., Liu, J. T., Huang, C., Selvaraj, K., et al. (2008). Detrital fine-grained sediment contribution from Taiwan to the northern South China Sea and its relation to regional ocean circulation. *Mar. Geol.* 255, 149–155. doi: 10.1016/j.margeo.2008.08.003

Liu, Z., Colin, C., Li, X., Zhao, Y., Tuo, S., Chen, Z., et al. (2010a). Clay mineral distribution in surface sediments of the northeastern South China Sea and surrounding fluvial drainage basins: Source and transport. *Mar. Geol.* 277, 48–60. doi: 10.1016/j.margeo.2010.08.010

Liu, Z., Li, X., Colin, C., and Ge, H. (2010b). A high-resolution clay mineralogical record in the northern South China Sea since the Last Glacial Maximum, and its time series provenance analysis. *Chin. Sci. Bulletin.* 55, 4058–4068. doi: 10.1007/s11434-010-4149-5

Liu, Z., Zhao, Y., Colin, C., Stattegger, K., Wiesner, M. G., Huh, C., et al. (2016b). Source-to-sink transport processes of fluvial sediments in the South China Sea. *Earth-Sci. Rev.* 153, 238–273. doi: 10.1016/j.earscirev.2015.08.005

Mahoney, J. B. (2005). Nd and Sr isotopic signatures of fine-grained clastic sediments: A case study of western Pacific marginal basins. *Sediment. Geol.* 182, 183–199. doi: 10.1016/j.sedgeo.2005.07.009

McDermott, F., Delfin, F. G., Defant, M. J., Turner, S., and Maury, R. (2005). The petrogenesis of volcanics from Mt. Bulusan and Mt. Mayon in the Bicol arc, the Philippines. *Contrib. Mineral. Petrol.* 150, 652–670. doi: 10.1007/s00410-005-0042-7

Meyer, I., Davies, G. R., and Stuut, J. W. (2011). Grain size control on Sr - Nd isotope provenance studies and impact on paleoclimate reconstructions: An example from deep - sea sediments offshore NW Africa. *Geochem. Geophys. Geosyst* 12. doi: 10.1029/2010GC003355

Milliman, J. D., Farnsworth, K. L., and Christina, S. A. (1999). Flux and fate of fluvial sediments leaving large islands in the East Indies. *J. Sea Res.* 41), 97–107. doi: 10.1016/s1385-1101(98)00040-9

Morley, C. K. (2012). Late Cretaceous–Early Palaeogene tectonic development of SE Asia. *Earth-Sci. Rev.* 115, 37–75. doi: 10.1016/j.earscirev.2012.08.002

Qiu, Z., Ma, W., Tao, C., Koschinsky, A., and Hu, S. (2022). Clay minerals and sr-nd isotope compositions of core CG 1601 in the northwest pacific: implications for material source and rare earth elements enrichments. *Minerals.* 12, 287. doi: 10.3390/min12030287

Qu, T., Girton, J., and Whitehead, J. (2006). Deepwater overflow through Luzon Strait. *J. Geophys. Res. Oceans* 111. doi: 10.1029/2005JC003139

Steinke, S., Chiu, H., Yu, P., Shen, C., Erlenkeuser, H., Loewemark, L., et al. (2006). On the influence of sea level and monsoon climate on the southern South China Sea freshwater budget over the last 22,000 years. *Quat. Sci. Rev.* 25, 1475–1488. doi: 10.1016/j.quascirev.2005.12.008

Steinke, S., Kienast, M., and Hanebuth, T. (2003). On the significance of sea - level variations and shelf paleo-morphology in governing sedimentation in the southern South China Sea during the last deglaciation. *Mar. Geol.* 201, 179–206. doi: 10.1016/S0025-3227(03)00216-0

Stevens, C. J., and Quinton, J. N. (2008). Investigating source areas of eroded sediments transported in concentrated overland flow using rare earth element tracers. *Catena.* 74, 31–36. doi: 10.1016/j.catena.2008.01.002

Sun, S., and McDonough, (1989). *Chemical and isotopic systematics of oceanic basalts: Implications for mantle composition and processes* Vol. 42) (London; Geological Society of London Special Publication), 313–345. doi: 10.1144/GSL.SP.1989.042.01.19

Syvitski, P. M. (2003). Supply and flux of sediment along hydrological pathways: research for the 21st century. *Glob. Planet. Change.* 39, 1–11. doi: 10.1016/S0921-8181(03)00008-0

Tam, T. A., Yumul, G. P., Ramos, E., Dimalanta, C. B., Zhou, M. F., and Suzuki, S. (2005). Rare earth element geochemistry of the Zigzag - Klondyke sedimentary rock formations: Clues to the evolution of the Baguio Mineral District (Luzon), Philippines. *Resour. Geol.* 55, 217–224.

Taylor, S. R., and McLennan, S. M. (1981). The composition and evolution of the continental crust: rare earth element evidence from sedimentary rocks. *Phys. Enginnering Sci.* 301, 381–399. doi: 10.1109/WFCS.2015.7160546

Wan, S., Li, A., Clift, P. D., and Jiang, H. (2006). Development of the East Asian summer monsoon: Evidence from the sediment record in the South China Sea since 8.5 Ma. *Palaeogeography Palaeoclimatology Palaeoecology.* 241, 139–159. doi: 10.1016/j.palaeo.2006.06.013

Wan, S., Toucanne, S., Clift, P. D., Zhao, D., Bayon, G., Yu, Z., et al. (2015). Human impact overwhelms long-term climate control of weathering and erosion in southwest China. *Geology.* 43, 439–442. doi: 10.1130/G36570.1

Wan, Z., Yao, Y., Chen, K., Zhong, S., Xia, B., and Sun, Y. (2019). Characterization of mud volcanoes in the northern Zhongjiannan Basin, western South China Sea. *Geol. J.* 54, 177–189. doi: 10.1002/gj.3168

Wang, A., Du, Y., Peng, S., Liu, K., and Huang, R. X. (2018). Deep water characteristics and circulation in the South China Sea. *Deep-Sea Res. Part I-Oceanogr. Res. Pap.* 134, 55–63. doi: 10.1016/j.dsr.2018.02.003

Wang, C., Liang, X., Foster, D. A., Liang, X., Tong, C., and Liu, P. (2019). Detrital zircon ages: A key to unraveling provenance variations in the eastern Yinggehai - Song Hong Basin, South China Sea. *Aapg Bull.* 103, 1525–1552. doi: 10.1306/11211817270

Wang, F., and Ding, W. (2023). How did sediments disperse and accumulate in the oceanic basin, South China Sea. *Mar. Pet. Geol.* 147. doi: 10.1016/j.marpetgeo.2022.105979

Wang, G., Xie, S., Qu, T., and Huang, R. X. (2011). Deep south China sea circulation. *Geophys. Res. Lett.* 38. doi: 10.1029/2010GL046626

Wang, W., Wang, X., Lu, Y., Li, S., Jin, J., Suo, Y., et al. (2024). Interaction between magmatism and polygonal faults revealed by three-dimensional seismic data in the Zhongjiannan Basin, South China Sea. *Mar. Pet. Geol.* 163, 106793. doi: 10.1016/j.marpetgeo.2024.106793

Wei, G., Liu, Y., Ma, J., Xie, L., Chen, J., Deng, W., et al. (2012). Nd, Sr isotopes and elemental geochemistry of surface sediments from the South China Sea: Implications for Provenance Tracing. *Mar. Geol.* 319, 21–34. doi: 10.1016/j.margeo.2012.05.007

Xu, Z., and Han, G. (2009). Rare earth elements (REE) of dissolved and suspended loads in the Xijiang River, South China. *Appl. Geochem.* 24, 1803–1816. doi: 10.1016/j.apgeochem.2009.06.001

Yang, S., Jiang, S., Ling, H., Xia, X., Sun, M., and Wang, D. (2007). Sr-Nd isotopic compositions of the Changjiang sediments: Implications for tracing sediment sources. *Sci. China Ser. D: Earth Sci.* 50, 1556–1565. doi: 10.1007/s11430-007-0052-6

Yang, S., Jung, H., Choi, M., and Li, C. (2002). The rare earth element compositions of the Changjiang (Yangtze) and Huanghe (Yellow) river sediments. *Earth Planet. Sci. Lett.* 201, 407–419. doi: 10.1016/S0012-821X(02)00715-X

Yang, S., Jung, H., Lim, D., and Li, C. (2003). A review on the provenance discrimination of sediments in the Yellow Sea. *Earth-Sci. Rev.* 63, 93–120. doi: 10.1016/S0012-8252(03)00033-3

Yang, Z., Jia, J., Wang, X., and Gao, J. (2013). Characteristics and variations of water and sediment fluxes into the sea of the top three rivers of Hainan in recent 50 years. *Mar. Sci. Bulletin.* 32, 92–99. doi: 10.11840/j.issn.1001-6392.2013.01.014

Yin, Z., Cai, Z., Yao, Y., Huang, Q., and Li, Z. (2023). Tectonic dynamics of the Zhongjiannan Basin in the western South China Sea since the late Miocene. *Front. Earth Sci.* 10. doi: 10.3389/feart.2022.996267

Zhang, L., Chen, M., Xiang, R., Zhang, L., and Lu, J. (2009). Productivity and continental denudation history from the South China Sea since the late Miocene. *Mar. Micropaleontol.* 72, 76–85. doi: 10.1016/j.marmicro.2009.03.006

Zhao, Z., Sun, Z., Wang, Z., Sun, Z., Liu, J., and Zhang, C. (2015). The high resolution sedimentary filling in Qiongdongnan Basin, Northern South China Sea. *Mar. Geol.* 361, 11–24. doi: 10.1016/j.margeo.2015.01.002